Deep Ocean storage of heat and CO_2 in the Fram Strait, Arctic Ocean during the last glacial period

Authors: Mohamed M. Ezat[1,2*], Tine L. Rasmussen[1], Mathis P. Hain[3], Mervyn Greaves[4], James W. B. Rae[5], Katarzyna Zamelczyk[1], Thomas M. Marchitto[6,7], Sönke Szidat[8,9], Luke C. Skinner[4]

[1] CAGE - Centre for Arctic Gas Hydrate, Environment and Climate, Department of Geosciences, UiT, The Arctic University of Norway, Norway.
[2] Department of Geology, Faculty of Science, Beni-Suef University, Beni-Suef, Egypt.
[3] Department of Earth and Planetary Sciences, University of California, Santa Cruz, CA, USA.
[4] Godwin Laboratory for Palaeoclimate Research, Department of Earth Sciences, University of Cambridge, UK.
[5] School of Earth & Environmental Sciences, University of St. Andrews, St. Andrews, United Kingdom.
[6] Department of Geological Sciences, University of Colorado Boulder, Boulder, CO, USA.
[7] Institute of Arctic and Alpine Research, University of Colorado Boulder, Boulder, CO, USA.
[8] Department of Chemistry, Biochemistry and Pharmaceutical Sciences (DCBP), University of Bern, Bern, Switzerland.
[9] Oeschger Centre for Climate Change Research (OCCR), University of Bern, Bern, Switzerland.

* Correspondence to: M. M. Ezat (mohamed.ezat@uit.no).

Key points

- Ambiguous interspecies differences in benthic foraminiferal $\delta^{18}O$ from the Nordic Seas for the last glacial maximum are due to bioturbation.
- Deep ocean temperature and $\delta^{18}O$ in central Fram Strait were ~1.5 °C and 1‰ higher during the last glacial maximum.
- Intermittent Nordic Seas outflow through Denmark Strait could have been the source of glacial North Atlantic water at 2000–3000 m water depth.

Abstract

The Fram Strait is the only deep gateway between the Arctic Ocean and the Nordic Seas and thus is a key area to study past changes in ocean circulation and the marine carbon cycle. Here, we study deep ocean temperature, $\delta^{18}O$, carbonate chemistry (i.e., carbonate ion concentration, [CO_3^{2-}]), and nutrient content in the Fram Strait during the late glacial (35,000–19,000 years BP) and the Holocene based on benthic foraminiferal geochemistry and carbon cycle modelling. Our results indicate a thickening of Atlantic water penetrating into the northern Nordic Seas, forming a subsurface Atlantic intermediate water layer reaching to at least ~2600 m water depth during most of the late glacial period. The recirculating Atlantic layer was characterized by relatively high [CO_3^{2-}] and low $\delta^{13}C$ during the late glacial, and provides evidence for a Nordic Seas source to the glacial North Atlantic intermediate water flowing at 2000–3000 m water depth, most likely via the Denmark Strait. In addition, we discuss evidence for enhanced terrestrial carbon input to the Nordic Seas at ~23.5 ka. Comparing our $\delta^{13}C$ and qualitative [CO_3^{2-}] records with results of carbon cycle box modelling suggests that the total terrestrial CO_2 release during this carbon input event was low, slow, or directly to the atmosphere.

1 Introduction

Late Pleistocene glaciations were characterized by millennial- and decadal- scale variations in global/regional climate and atmospheric carbon dioxide levels (i.e., pCO_2), superimposed on gradual longer-term trends of increasing ice volume and decreasing atmospheric pCO_2 (e.g., Bard et al., 1990; Barker et al., 2011; Marcott et al., 2014; Bereiter et al., 2015). For example, Greenland ice core records show that the high latitude North Atlantic region underwent ~25 millennial-scale climate oscillations during the last glacial period

(~110,000–19,000 years ago; 110–19 ka), referred to as Dansgaard-Oeschger (DO) events (Dansgaard et al., 1993). These DO events, consisting of warm interstadials and cold stadials, are characterized by an abrupt atmospheric warming over Greenland of 8–16 °C from cold stadials to warm interstadials followed by a gradual cooling and eventually a sudden cooling back to stadial conditions (Huber et al., 2006). Associated with DO events, high-resolution records of atmospheric pCO_2 from Antarctic ice cores reveal millennial-scale (up to 25 ppm) and centennial-scale (up to 10 ppm) variations (e.g., Marcott et al., 2014; Bereiter et al., 2015; Bauska et al., 2018).

The Atlantic Meridional Overturning Circulation (AMOC), which is a crucial regulator of the earth's climate variability, is thought to have played a leading role in these (sub)millennial-scale variations in climate and atmospheric pCO_2 through its control on heat redistribution and ocean-atmosphere gas exchange (e.g., Broecker, 1998; Fischer et al., 2010). Modern exchange of surface and deep water between the Arctic Ocean, the Nordic Seas and the North Atlantic Ocean represents the northern limb of the AMOC (Hansen and Østerhus, 2000). Northward inflow of warm Atlantic water across the Greenland-Scotland ridge advects heat, salt and carbon to the Nordic Seas and the Arctic Ocean, where the major part of the inflow water densifies and returns as deep overflows to the North Atlantic (Hansen and Østerhus, 2000). The evolution of this circulation pattern during the last glacial period and its contribution to glacial climate and atmospheric pCO_2 variations is still elusive. For example, deep ocean exchanges between the Arctic Ocean and the Nordic Seas are particularly poorly constrained during the Last Glacial Maximum (LGM; 25–19 ka), when global ice sheets reached their maximum integrated volume (e.g., Clark et al., 2010). Moreover, carbon exchanges between the deep ocean, the surface ocean and the atmosphere are even less constrained in the Arctic Ocean and Nordic Seas for the last glacial period. This is partly due to limited availability of deep-sea sediments dating from the LGM from the central Arctic

Ocean, because of extensive sea ice cover resulting in very low or no sedimentation (e.g., Hanslik et al., 2010). In addition, $\delta^{18}O$ values measured in benthic foraminifera from the deep northern and central Nordic Seas show large and ambiguous interspecies differences (Bauch et al., 2001; Ezat et al., 2019).

The Fram Strait is an important gateway between the Arctic Ocean and the Nordic Seas and thus is a key area to investigate the heat and carbon exchanges between the Arctic Ocean, the Nordic Seas and the Atlantic Ocean. In addition, marine records from the deep Fram Strait document enhanced flux of terrestrial carbon to the northern Nordic Seas at ~24 ka (Hebbeln et al., 1994). Changes in terrestrial carbon storage have also been suggested to have played a role in some abrupt centennial-scale changes in atmospheric pCO_2 (e.g., Bauska et al., 2016). Given the vast and dynamic permafrost and subglacial carbon reservoirs in the Arctic region (e.g., Vonk et al., 2012; Tarnocai et al., 2009; Köhler et al., 2014; Wadham et al., 2019; Meyer et al., 2019), and the increased melting and release of huge icebergs from surrounding ice sheets (e.g., Luckman et al., 2006; Bjørk et al., 2012; Mankoff et al., 2020), it is imperative to study the impact of a possible 'terrestrial carbon mobilization' event at ~24 ka on deep ocean carbonate chemistry and atmospheric pCO_2.

Here, we assess the interspecies differences in benthic foraminiferal $\delta^{18}O$ and study the glacial evolution of deep-ocean temperatures, $\delta^{18}O$ and carbonate chemistry in the deep, central Fram Strait (~2600 m water depth) for the 35–19 ka period using benthic foraminiferal element/Ca, radiocarbon and isotope measurements from two deep ocean sediment cores (~2600 m water depth). In addition, we use the CYCLOPS carbon cycle box model to assess the effects of a possible 'terrestrial carbon mobilization' event at ~24 ka on atmospheric pCO_2 and the carbonate chemistry of the deep 'Northern Component Water', and compare the model results with our proxy reconstructions. The overall purpose is to study the exchange of deep water through the Fram Strait and explore the contribution of ocean circulation and

biogeochemical changes in the northern Nordic Seas to glacial climate and carbon cycle variations.

2 Material and methods

This study is based on new and published data from two sediment cores HH12-946MC (78°53' N; 01°45' W; 2637 m water depth) and HH12-948MC (78°52' N; 00°21' E; 2542 m water depth) from the central Fram Strait (Ezat et al., 2019; Figure 1). Published results from sediment cores HLY0503-18TC (88°45' N; 146°68' E; 2654 m water depth; Cronin et al., 2012), PS1243 and MD99-2276 (69°37' N, 06°55' W, 2711 m water depth; Bauch et al., 2001; Thornalley et al., 2015), 1294-4 (77° 59.9' N; 5°22.3' E; 2668 m water depth; Hebbeln et al., 1994), 1295-5 (77°59.2' N; 2°24.8' E; 3112 m water depth; Hebbeln et al., 1994), and HM52-43 (64° 25' N, 0.73° E, 2781 m water depth; Veum et al., 1992) are also closely compared and discussed (Figure 1).

2.1 Stable carbon and oxygen isotopes

We use published foraminiferal $\delta^{18}O$ and $\delta^{13}C$ records of the planktic species *Neogloboquadrina pachyderma*, the shallow infaunal benthic species *Oridorsalis umbonatus* and the epifaunal benthic species *Cibicidoides wuellerstorfi* from cores HH12-946MC and HH12-948MC (Ezat et al., 2019). In order to increase the temporal resolution and extend the investigated time interval, new measurements were obtained on *O. umbonatus* following the methods described in Ezat et al. (2019).

In addition, new stable isotope measurements on *C. wuellerstorfi* from core HH12-948MC were made after acid leaching. About 6 specimens of *C. wuellerstorfi* were crushed and leached by 0.01M HCl for 15 minutes, including ultrasonication for 5 minutes. Thereafter, the samples were rinsed immediately by milliQ water. The $\delta^{18}O$ and $\delta^{13}C$ were

then measured at the Godwin Laboratory for Paleoclimate Research, University of Cambridge, UK. These new measurements were performed to investigate the possibility that the low $\delta^{18}O$ previously recorded in *C. wuellerstorfi* (Bauch et al., 2001; Thornalley et al., 2015; Ezat et al., 2019) could be caused by diagenetic coating with extremely low $\delta^{18}O$. It was not possible to perform this 'acid leaching' test on core HH12-946MC, because all specimens of *C. wuellerstorfi* in this core were already used for stable isotope analyses and radiocarbon dating (see below).

2.2 Benthic element/Ca analyses and seawater temperature and $\delta^{18}O_{water}$ calculations

For element/Ca analyses, we used the most persistent and abundant benthic foraminiferal species in our study region, *O. umbonatus* (Bauch et al., 2001; Ezat et al., 2019). A total of 25 to 30 pristine specimens of *O. umbonatus* were carefully picked from the 150–250 µm size fraction from sediment cores HH12-948MC and HH12-946MC. After crushing, the samples were cleaned following the reductive-oxidative method described in Pena et al. (2005) and originally published in Boyle and Keigwin (1985). At the day of analyses, the samples were dissolved using 330 µl 0.1M HNO_3. After centrifugation for 5 minutes (7000 rpc), 300 µl of the samples were transferred to new acid-cleaned vials. For blank samples (which have been treated with cleaning reagents as actual samples), 50 µl of a high purity 2000 ppm Ca^{2+} solution was added before adding the acid, to enable determination of the blanks as element/Ca. An aliquot of 50 µl of each sample was added to 200 µl 0.1M HNO_3 and analyzed on an ICP-OES to determine their [Ca^{2+}]. Accordingly, the samples were re-diluted to 10 ppm [Ca^{2+}] using '0.3M HF - 0.1M HNO_3' mixture and were analyzed by HR-ICP-MS at the University of Cambridge following Misra et al. (2014). Based on repeated measurements of in-house standard solutions (n=11), the analytical precision (2 sd) for both B/Ca and Mg/Ca is 0.9%. Blank samples (n=9) show average B/Ca and Mg/Ca of 2.5

160 µmol/mol and 0.027 mmol/mol, respectively, suggesting insignificant contamination from
161 vials or cleaning/dissolution reagents. Mn/Ca, Fe/Ca (except two samples) and Al/Ca (except
162 four samples) are < 25 µmol/mol, 50 µmol/mol and 50 µmol/mol respectively, indicating
163 negligible contamination by terrigenous materials or diagenetic coatings (e.g., Barker et al.,
164 2005).

165 Mg/Ca was converted to bottom water temperature (BWT; °C) using the equation
166 from Barrientos et al. (2018): (*O. umbonatus* Mg/Ca = A * exp(0.102 ± 0.01*BWT). The pre-
167 exponential constant (A) is calibrated to our core-top samples from core HH12-948MC
168 (which are <2000 years BP) yielding a value of 1.45. Elderfield et al. (2006) has shown that
169 Mg/Ca data of *O. umbonatus* from sites with BWT <2 °C do not follow a simple calibration
170 curve. This could be related to the 'carbonate ion' effect (e.g., Elderfield et al., 2006), partial
171 dissolution, and/or use of a wide size range of foraminiferal specimens (e.g., Tisserand et al.,
172 2013). Nevertheless, the consistency between published BWT reconstructions based on
173 Mg/Ca measurements of *O. umbonatus* and independent BWT reconstructions from clumped
174 isotopes (Thornalley et al., 2015) and Mg/Ca measured on ostracods (Cronin et al., 2012)
175 from the central Nordic Seas (see Thornalley et al., 2015) provides confidence in the use of
176 this species in BWT reconstructions in our study region.

177 Seawater $\delta^{18}O$ was calculated by removing the temperature component of the $\delta^{18}O$-*O.*
178 *umbonatus* using the equation from Shackleton (1974). To convert from the Pee Dee
179 Belemnite scale for carbonate $\delta^{18}O$ to Standard Mean Ocean Water for $\delta^{18}O$-water, 0.2 was
180 added (Shackleton, 1974). Using other available equations (Bemis et al., 1998; Marchitto et
181 al., 2014) would change the amplitude of glacial-interglacial change in seawater $\delta^{18}O$ by
182 <0.1‰.

183

184 **2.3 Radiocarbon analyses**

185 Four ^{14}C dates from core HH12-946MC on specimens of *C. wuellerstorfi* (~ 250–
186 600 µg carbonate per sample) were measured following Gottschalk et al. (2018) using the
187 Mini Carbon Dating System (MICADAS) at the University of Bern (Szidat et al., 2014). In
188 brief, foraminiferal samples were loaded into septum-sealed glass vials. The air in the vials
189 was removed and replaced by He using two concentric needles inserted through the septum by
190 the automated carbonate handling system. The foraminiferal samples were then weakly
191 leached by adding 200 µl 0.01 M HCl for 3 min at room temperature. After a second flush of
192 the vials with He (to remove CO_2 produced during leaching), 0.5 mL 85% (~ 15 M)
193 orthophosphoric acid (H_3PO_4) was added with a gas-tight syringe for carbonate dissolution.
194 The reaction was run to completion over night at a temperature of 70°C. To evaluate possible
195 methodological bias when comparing between 'MICADAS-based' *C. wuellerstorfi* and
196 published 'graphitization-based' *O. umbonatus* and *N. pachyderma* ^{14}C dates measured at the
197 ^{14}Chrono Centre, Queen's University Belfast, Northern Ireland (Ezat et al., 2019), one *N.*
198 *pachyderma* ^{14}C date was measured by MICADAS following the methods outlined above.
199 The MICADAS-based *N. pachyderma* date is consistent with 'graphitization-based' *N.*
200 *pachyderma* dates (Table 1; Supplemental Figure 1), indicating negligible methodological
201 bias.
202
203 **2.4 Age models**
204 The age models of cores HH12-946MC and HH12-948MC have been published
205 previously (Ezat et al., 2019) and are based on calibrated planktic ^{14}C dates (Supplemental
206 Tables 2, 3) using the Marine13 dataset in Calib 7.04 (Reimer et al., 2013). Here we update
207 the age models using the recently published Marine20 dataset (Heaton et al., 2020) in Calib
208 8.2 (Stuiver et al., 2020) (Tables S1, S2). We used ΔR (the regional difference from the
209 average global marine reservoir correction) = 1000 years (i.e., reservoir age = ~1500 years)

for the glacial parts of the records and ΔR=0 for the Holocene. Although changes in the reservoir age in the Fram Strait during the last glacial period remain unconstrained, the assigned value of 1500 ^{14}C years are consistent with reservoir age estimates from the southern and central Norwegian Sea (Thornalley et al., 2015; Ezat et al., 2017) as well as with modelling results (e.g., Butzin et al., 2020). The resulting sedimentation rates range from 0.6 to 9 cm/kyr in core HH12-946MC, with an average of 2 cm/kyr for both the Holocene and glacial parts (Tables S1, S2). These relatively low sedimentation rates can potentially induce large smoothing effects from bioturbation. However, because the ^{14}C dates of *N. pachyderma* and *O. umbonatus* are in chronological for the glacial part of the record, and because ^{14}C dates of *O. umbonatus* are older than those of *N. pachyderma* (except for one sample at 28.25 cm, but the difference is less than the analytical uncertainty; Table 1), we conclude that the impact of burrowing activity is minor. Furthermore, our study mainly target the relatively long-term changes from late MIS 3 to LGM. According to the age model, the transition from late MIS3 to the LGM is characterized by a pronounced increase in δ^{18}O values measured in *N. pachyderma* and *O. umbonatus* (Ezat et al., 2019; see also 'Results and Discussion' section), which provides confidence in our age model at such timescales.

The original age models of sediment cores 1294, 1295 from the eastern Fram Strait were based on uncorrected planktic radiocarbon dates (Hebbeln et al., 1994). We updated the original age models of cores 1294, 1295 by the same approach as for cores HH12-946MC and HH12-948MC (Tables S3, S4). The age models of sediment cores PS1243 and MD99-2276 from the central Nordic Seas were based on correlation to the well-dated sediment cores from the southern Norwegian Sea (see Rasmussen and Thomsen, 2004; Ezat et al., 2017) using the planktic δ^{18}O (Thornalley et al., 2015). Unfortunately, because of missing data from the deglaciation, the planktic δ^{18}O records from the Fram Strait cannot be correlated with the

234 records from the southern Norwegian Sea. Finally, in this study, we define a Heinrich stadial
235 as the whole stadial period during which a Heinrich event occurred (e.g., Barker et al., 2011).

236

237

238 **2.5 Carbon cycle modelling**

239 Given the evidence of an abrupt +10 ppm jump in atmospheric CO_2 (e.g., Ahn and
240 Brook, 2014; Bereiter et al., 2015) and an enhanced influx of terrestrial carbon to the Nordic
241 Seas (Hebbeln et al., 1994) at the Heinrich Stadial 2/Interstadial 2 transition (~23.5 ka), we
242 are interested if and how the 'mobilization of terrestrial carbon' could be recorded in
243 'Northern Component Water'. For this, we used the glacial configuration of the CYCLOPS
244 carbon cycle box model (Hain et al., 2010, 2014) as a point of comparison to our
245 observational records and in order to assess the effects of possible mobilization of terrestrial
246 carbon at this time. The baseline model scenario is spun-up to the reference LGM conditions,
247 including Southern Ocean changes that dominated simulated glacial CO_2 drawdown (Hain et
248 al., 2010; Sigman et al., 2010), as well as a 'Glacial North Atlantic Intermediate Water'
249 (GNAIW; e.g., Lynch-Stieglitz et al., 2007) representation of the AMOC that is needed to
250 account for the gross pattern of LGM and deglacial carbon isotope changes (Sigman et al.,
251 2003; Hain et al., 2014). The GNAIW configuration in CYCLOPS has the same 21.5 Sv
252 strength (1 Sv = 10^6 m^3/s) as the default NADW configuration, but the lower limb of the
253 southward return flow is restricted to mid-depth as opposed to present-day NADW flowing in
254 the deep Atlantic basin. This initial steady state of the model is perturbed with a sequence of
255 Atlantic circulation changes that is designed to mimic the Heinrich stadial 2/interstadial 2
256 transition changes; starting with GNAIW, switching to a 'Heinrich Stadial' collapsed state of
257 the AMOC for the duration of Heinrich stadial 2 (4000 years), followed by the default
258 NADW circulation to represent vigorous and deep overturning during interstadial 2 (1300

years), and finally a return to the initial GNAIW circulation. This treatment is equivalent to the representation of the deglacial AMOC changes described in Hain et al. (2014). Assuming these simplistic 'ad hoc' changes adequately reflect Atlantic changes over the Heinrich stadial 2/interstadial 2 interval, the simulated biogeochemical changes in the "Northern Component Water" model reservoir, which represents the subsurface high-latitude North Atlantic including the Nordic Seas, serve as a comparison baseline for our observational data. To simulate the spectrum of hypotheses of how terrestrial carbon may have been mobilized from the largely glaciated high-northern continents we consider both (1) oxidation on land with CO_2 release directly to the atmosphere, and (2) erosion and transfer of terrestrial carbon to the deep Nordic Seas/Arctic Ocean (as represented by the 'Northern Component Water'). In each of these two pathway cases, we simulate 100-year mobilization events incrementing the total amount of carbon released from zero to 88 Pg C (1 Pg C = 10^{15} gram carbon), similar to the experiments of Köhler et al. (2011, 2014) where 125 Pg C from land was released to the atmosphere at 14.6 ka within a time window of 50 to 200 years. In this paper, we only discuss the results from the carbon addition experiments. For a summary of the results from idealized circulation scenarios, see Text S1 (Supporting Information).

3 Results and Discussion

3.1 Interspecies benthic foraminiferal $\delta^{18}O$ differences and implications

One significant obstacle to reconstruct deep ocean conditions in the northern and central Nordic Seas for the last glacial period is the ambiguous large $\delta^{18}O$ differences between the epifaunal benthic foraminiferal species *C. wuellerstorfi* and the shallow infaunal species *O. umbonatus* (Bauch et al., 2001; Thornalley et al., 2015; Ezat et al., 2019). Epifaunal $\delta^{18}O$ is ~1‰ lower than coeval infaunal $\delta^{18}O$ from sediments dated to the LGM (Figure 2). In

addition, the epifaunal $\delta^{18}O$ from the LGM sediments is up to 1‰ lower compared to the Holocene, which is in contrast to all other ocean basins and the SE Norwegian Sea (Figure 2). It has been suggested that this low epifaunal $\delta^{18}O$ from the LGM sediments indicates short-term, but regional ventilation events by brine formation (Bauch et al., 2001). However, it remains possible that *C. wuellerstorfi* specimens were transported from younger/shallower sediments or have a diagenetic carbonate coating with very low $\delta^{18}O$. Our results show that intensive acid leaching before $\delta^{18}O$ measurements (see Methods) did not change the $\delta^{18}O$ values (Figure 2d). Thus, we can here eliminate the possibility that the low *C. wuellerstorfi* $\delta^{18}O$ values are due inorganic carbonate coatings.

Radiocarbon dating of *C. wuellerstorfi* could reveal whether these *C. wuellerstorfi* specimens are autochthonous. The abundance of *C. wuellerstorfi* in the glacial sediments from the central and northern Nordic Seas is very low (~<5% of the benthic foraminiferal assemblages compared to 40% during the Holocene) with an average of 7 specimens per sample (~300 µg carbonate) (Bauch et al., 2001; Ezat et al., 2019). Our MICADAS ^{14}C dates, obtained on small samples of *C. wuellerstorfi* from the LGM sediments, range from 14,000 to 15,400 ^{14}C years BP. Furthermore, they date ~ 4500 ^{14}C years younger than the ages obtained on coeval *O. umbonatus* and *N. pachyderma* (Figure 2c, Table 1). This clearly indicates that these *C. wuellerstorfi* specimens are not of LGM age and that the specimens probably have been reworked from younger sediments. These results confirm that caution is needed when using low abundant 'proxy carriers' from low sedimentation rate areas (c.f., Peng and Broecker, 1984). However we also note that down-mixing of Holocene specimens cannot fully explain the young ages of *C. wuellerstorfi* because $\delta^{18}O$ values in *C. wuellerstorfi* from the LGM sediments are even lower than those from the Holocene. The deglacial sediments in our two records from the central Fram strait are barren of calcareous foraminifera, which have been attributed to either post-depositional dissolution or unfavourable conditions (Zamelczyk

et al., 2014; Ezat et al., 2019). If post-depositional dissolution was the reason for the absence of foraminifera in the deglacial sections of our Fram Strait cores, an earlier downcore mixing of deglacial foraminifera with very low $\delta^{18}O$ (typical of HS1 in this region) into the LGM sediments may have occurred. However, we emphasize that the reworking process of *C. wuellerstorfi* into the LGM sediments remains not fully explained.

Regardless of the transport mechanism of younger *C. wuellerstorfi* into the LGM sediments in the deep Fram Strait, it is clear that the geochemical signals in *C. wuellerstorfi* (e.g., $\delta^{18}O$ and $\delta^{13}C$) cannot be used in this context to infer hydrographic and ventilation changes in the region during the LGM. Given the striking similarity of $\delta^{18}O$ measured in *C. wuellerstorfi* from LGM sediments in the Fram Strait (Ezat et al., 2019; this study) and the central Nordic Seas (Bauch et al., 2001) (Figure 2), our results suggest that inferences of the ocean circulation during the LGM based on $\delta^{18}O$ and $\delta^{13}C$ in *C. wuellerstorfi* from the central Nordic Seas (e.g., Bauch et al., 2001; Thornalley et al., 2015; Knies et al., 2018; Mackensen and Schmiedl, 2019) also should be treated with caution. Radiocarbon dating of the *C. wuellerstorfi* from the central Nordic Seas could settle the issue about reworking. We thus base our reconstructions of ocean circulation and carbonate chemistry in the northern Nordic Seas on shell geochemistry of *O. umbonatus*.

It is also notable that $\delta^{18}O$ of *C. wuellerstorfi* from the deep southern Norwegian Seas do not show the same low values for the LGM and that $\delta^{18}O$ values of both *C. wuellerstorfi* and *O. umbonatus* are consistently high (Veum et al., 1992) (Figure 2b) similar to *O. umbonatus* $\delta^{18}O$ from the central and northern Nordic Seas (Figure 2). This provides confidence in using *C. wuellerstorfi* geochemistry from LGM sediments from the southern Norwegian Sea records, in contrast to the northern (and likely central) Nordic Seas deep records.

3.2 Deep temperature and $\delta^{18}O$ evolution

Our BWT reconstructions from ~2600 m water depth from the central Fram Strait based on Mg/Ca in *O. umbonatus* varies between -0.2 and 1°C during MIS 3 (~40–26 ka) with an average of 0.6±0.5 °C (Figure 3b). This is ~1.5±0.5 °C warmer than the modern and average Holocene temperatures, which are ~-0.8 °C (Figure 3b). These BWT changes are in agreement with those from the central Arctic Ocean at the same water depth based on Mg/Ca in ostracods (Cronin et al., 2012) (Figure 3). Our BWT record further shows an increasing trend along the transition from MIS 3 to the LGM with the highest BWT (~1.2 °C) recorded at ~26–24 ka (Figure 3b). At ~23.5 ka, close to the timing of interstadial 2, the BWT decreased to ~0 °C and thereafter it fluctuated between ~0 and 0.5 °C at 22–20 ka (Figure 3b).

Deep benthic foraminiferal $\delta^{18}O$ records from the Nordic Seas (excluding epifaunal records from the central and northern Nordic Seas; see section 3.1) reveal a glacial-interglacial change of only 0.7‰ (Figure 2; 3a), which is smaller than records from other ocean basins. Our deep-water $\delta^{18}O$ estimates based on $\delta^{18}O$ and temperature correction using Mg/Ca in *O. umbonatus* shows a 1‰ glacial-interglacial change, which is similar to the estimated global average ocean $\delta^{18}O$ change (Figure 3d). Seawater $\delta^{18}O$ in the deep Nordic Seas increased from 0.7‰ during late MIS 3 to 1‰ during the LGM (Figure 3d). This pattern mimics the global ocean changes in deep-water $\delta^{18}O$ (Figure 3d). The consistent amplitude and evolution of seawater $\delta^{18}O$ variations in the Nordic Seas (and possibly the central Arctic Ocean) and the mean global ocean change are in agreement with persistent exchange of deep water with other ocean basins (though likely with different modes and rates) and argue against extreme isolation of the Arctic Ocean. This is consistent with the new ^{14}C-based evidence from the Fram Strait (Ezat et al., 2019). Based on the previously inferred 'stagnation' of the deep Arctic Ocean and the Nordic Seas (ventilation ages up to 10,000 years), geothermal heating was suggested as a significant contributor to the glacial deep ocean warming in the

region (Thornalley et al., 2015). In contrast, recent ^{14}C evidence from the Fram Strait (Ezat et al., 2019) and our deep-water $\delta^{18}O$ evolution (Figure 3d) suggest smaller ventilation ages and more exchange with other ocean basins, which would have limited the contribution of geothermal heating to the deep-water warming. We propose that these observations can be reconciled if the glacial warming observed in the Nordic Seas is attributed instead to thickening and/or deepening of the Atlantic intermediate water, allowing it to influence deeper areas than at present. This also suggests a significant reduction and/or shoaling of cold deep water formation by open ocean convection. Planktic $\delta^{18}O$ records from the Nordic Seas display an increase from the southern Norwegian Sea (64° 25' N), central Nordic Seas (69°37' N) to the Fram Strait (78°53' N) during the Holocene (Figure 3e), which likely reflects the cooling of the Atlantic water as it flows northward. This gradient is largely diminished during the glacial period in particular at 22–19 ka (Figure 3) probably suggesting overall colder sea surface temperatures in the region and a dominant subsurface flow (and thus negligible heat loss) instead of a surface flow subject to air-sea exchange.

3.3 Carbonate chemistry and $\delta^{13}C$ records

Epifaunal benthic foraminiferal geochemistry is typically used to reconstruct deep ocean chemistry changes (e.g., Duplessy et al., 1988; Yu and Elderfield, 2007; Mackensen and Schmiedl, 2019). Given the reworking problem that we identify with the available epifaunal species (*C. wullerstorfi*) from the glacial sediments in our study area (see section 3.1), we instead use $\delta^{13}C$ and B/Ca measured in the shallow infaunal benthic foraminiferal species *O. umbonatus* for the reconstruction of carbonate chemistry changes. In the North Atlantic Ocean, *O. umbonatus* lives in the upper 1 cm of the sediments (Corliss, 1985), which may indicate influence from pore water chemistry. However, the overall low productivity and supply of carbon to the deep sea as well as low sediment accumulation rates in the Fram Strait

likely suggest insignificant decoupling between bottom water and shallow (< 2 cm deep in the sediments) pore water chemistry. In addition, the central Arctic Ocean equivalent of *O. umbonatus* (*O. tener*) is considered to have an epifaunal microhabitat (Murray, 2006; Barrientos et al. 2018). In general, B/Ca in benthic foraminifera, including infaunal species, show a positive correlation with the deep-water carbonate saturation ($\Delta[CO_3^{2-}]$), providing a method for the reconstruction of deep-ocean carbonate ion concentration ($[CO_3^{2-}]$) (Yu and Elderfield, 2007; Yu et al., 2008; Rae et al., 2011). Carbonate ion concentration broadly records the difference or ratio between the two master variables of the carbonate system, Alkalinity and Dissolved Inorganic Carbon (DIC), allowing $[CO_3^{2-}]$ reconstructions to inform on past changes in carbon storage in the ocean (Broecker and Peng, 1982; Yu et al., 2008, 2016). Thus, we use *O. umbonatus* B/Ca and $\delta^{13}C$ as qualitative indicators of $[CO_3^{2-}]$ and nutrients, respectively. Given the shallow infaunal habitat of *O. umbonatus*, this should nonetheless be taken with caution.

The B/Ca in *O. umbonatus* increased from ~52 µmol/mol during late MIS 3 to ~ 62 µmol/mol during the LGM and subsequently decreased to ~43 µmol/mol during the Holocene (Figure 4b). This suggests higher glacial $[CO_3^{2-}]$, with highest values during the LGM as seen in many studies for mid-depth records from the North Atlantic Ocean (Yu et al., 2008, 2010, 2020). The $\delta^{13}C$ in the infaunal species *O. umbonatus* is on average ~1‰ lower during the last glacial (~40–19 ka) compared to the Holocene (Figure 4e). The glacial-interglacial changes in $\delta^{13}C$ and B/Ca of *O. umbonatus* are generally consistent with $\delta^{13}C$ and B/Ca in *C. wuellerstorfi* from the subpolar North Atlantic Ocean at water depths between 2000 and 3000 m (Yu et al., 2008) (Figure 4). This supports the inference of Yu et al. (2008) that the Nordic Seas have contributed to the lower glacial North Atlantic intermediate water (LGNAIW) water mass. Idealized numerical modelling shows that under extensive sea-ice cover and subsurface inflow of Atlantic water into the Nordic Seas, Atlantic water recirculates as a

western boundary current out of the Nordic seas (Jensen et al., 2018). The Denmark Strait may therefore have provided an overflow pathway of the subsurface Atlantic water to the North Atlantic Ocean.

3.4 Changes in the terrestrial carbon input and carbon cycle modelling

During the later part of Heinrich stadial 2 and the transition to interstadial 2, $\delta^{13}C$ of organic material and C/N from three nearby records show a significant and relatively abrupt decrease suggesting an increase in the input of terrestrial carbon (Hebbeln et al., 1994; see Figure 4d). This is associated with a decrease in $\%CaCO_3$ and an increase in Ice Rafted Debris (IRD) (Hebbeln et al., 1994). Although a limited number of records of $\delta^{13}C$ measured in organic material are available from the region (Hebbeln et al., 1994), the decrease in $\%CaCO_3$ and increase in IRD close to the end of Heinrich stadial 2 are widely recorded from the northern Nordic Seas (e.g., Jessen et al., 2010; Zamelczyk et al., 2014) and suggest that the increase in the input of terrestrial carbon was probably a geographically wide-spread feature. This possibly hints to a mobilization event of Arctic permafrost and/or carbon release from ice sheets. Arctic permafrost, which can be divided into terrestrial (~1,000 Pg C), ice complex (~400 Pg C) and subsea (~1,400 Pg C) permafrost, is a major active component of the global carbon cycle (e.g., Tarnocai et al., 2009; Vonk et al., 2012). Also, ice sheets represent an interactive player in the global carbon cycle (e.g., Wadham et al., 2019). Within the limitation of our chronology due to uncertainty about past changes in R (section 2.4), this event may have occurred sometime between 24.5 ka and 23 ka. We do not have constraints on the source, magnitude or transport pathways of this possible ‘terrestrial carbon’ mobilization event. However, some of this mobilized carbon likely entered the atmosphere directly, while a smaller part entered the Arctic Ocean system.

Although ocean biological and physical processes have likely been leading mechanisms for the glacial/interglacial and millennial-scale variations in atmospheric pCO_2, and may contribute to centennial-scale changes (e.g., Ezat et al., 2017; Rae et al., 2018), oxidation of terrestrial organic carbon may also have played a role in abrupt centennial-scale events (e.g., Köhler et al., 2014; Bauska et al., 2016; Meyer et al., 2009). Given the evidence of an abrupt increase of 10 ppm in atmospheric CO_2 (e.g., Bereiter et al., 2015) and an enhanced influx of terrestrial carbon to the Nordic Seas (Hebbeln et al., 1994) at the Heinrich stadial 2/interstadial 2 transition, we are interested in finding out if and how the mobilization of terrestrial carbon in the northern high latitudes is recorded in the deep 'Northern Component Water'. To test the relative sensitivity of atmospheric pCO_2 and 'Northern Component Water' carbonate chemistry, we superimpose two sets of carbon mobilization scenarios onto the CYCLOPS model idealized circulation scenario, with one set adding respired carbon directly to the atmosphere (Figure 5, left panel) or alternatively directly to 'Northern Component Water' (Figure 5, right panel). In both cases, carbon is added for 100 years with cumulative mobilization ranging 0–88 Pg C for individual realizations. If ~45 Pg C are directly released to the atmosphere, simulated atmospheric pCO_2 experiences an abrupt and short-lived 10 ppm increase, similar to reconstructions of interstadial 2 (Figure 4g). In all cases where the carbon is added to the atmosphere the global surface ocean immediately absorbs about half of the added carbon and the associated ocean acidification and Suess effect are dispersed and not concentrated near the boreal source and 'Northern Component Water'. The carbonate chemistry and $\delta^{13}C$ of DIC remain principally controlled by large-scale changes in ocean circulation, and not by the carbon addition. In contrast, if the carbon is released to the 'Northern Component Water', the model predicts abrupt and severe decline of $[CO_3^{2-}]$ and $\delta^{13}C$ of DIC in the 'Northern Component Water' because the carbon becomes concentrated in the interior Atlantic rather than dispersed globally. For that reason carbon release to the

457 'Northern Component Water' is unlikely to result in a transient atmospheric pCO_2 spike. It is
458 expected that the anomalies in $[CO_3^{2-}]$ and $\delta^{13}C$ of DIC in the 'Northern Component Water'
459 depend on the rate of carbon release because with NADW circulation during interstadial 2, the
460 water residence time in the 'Northern Component Water' is short and advection and
461 dissipation of the added carbon to the global deep ocean is facilitated by the vigorous AMOC.
462 From these idealized carbon mobilization scenarios, we conclude that carbonate chemistry
463 and $\delta^{13}C$ from the Nordic Seas should be relatively sensitive to respiration of terrestrial
464 organic matter at depth, where carbon remains relatively concentrated until ocean circulation
465 dissipates the added carbon. This pathway of carbon mobilization has only a minimal
466 transient effect on atmospheric pCO_2 because the carbon is initially concentrated and then
467 dissipated within the ocean interior. The alternative pathway, direct release to the atmosphere,
468 causes an immediate CO_2 transient that is moderated by the global surface ocean Revelle
469 buffer factor and its total buffer capacity, with the global dispersion of the added carbon
470 precluding the generation of significant regionally focused carbonate chemistry anomalies.
471 We only observe modest changes in our B/Ca and $\delta^{13}C$ records at the Heinrich stadial
472 2/interstadial 2 transition (Figure 4b,c). Thus, if the terrestrial organic matter influx at
473 Heinrich stadial 2/interstadial 2 (Hebbeln et al., 1994; Figure 4) recorded a mobilization event
474 of subglacial or permafrost carbon, the total carbon release was likely low or slow, or released
475 directly to the atmosphere.

476

477 **4. Conclusions**

478 In this study, we reconstructed deep ocean hydrographic changes in the northern
479 Nordic Seas during the late glacial (35–19 ka). Furthermore, we investigated the ambiguously
480 large differences of $\delta^{18}O$ between two benthic foraminiferal species *Oridorsalis umbonatus*

(shallow infaunal) and *Cibicidoides wuellerstorfi* (epifaunal) that have been recorded from sediments dating from the last glacial maximum (LGM) in the central and northern Nordic Seas. Using species-specific foraminiferal ^{14}C dating, we showed that the specimens of *C. wuellerstorfi* have been reworked. We therefore based our reconstructions on the most persistent and abundant benthic species *O. umbonatus*. We propose that the reconstruction of glacial ocean circulation in low-resolution deep-sea sediments from this region based on $\delta^{18}O$ and $\delta^{13}C$ measured in *C. wuellerstorfi* should be treated with caution.

Our bottom water temperatures (BWT) from Mg/Ca show, in agreement with previous studies from the Arctic Ocean and central Nordic Seas, that the deep northern Nordic Seas were on average 1.5 °C warmer during the late glacial compared to the Holocene. Furthermore, local (and potentially regional) seawater $\delta^{18}O$ was 0.7 and 1‰ higher during late MIS 3 and the LGM, respectively, relative to the Holocene. The similarity in the magnitude and evolution between our seawater $\delta^{18}O$ record and global average ocean $\delta^{18}O$ supports the recent ^{14}C evidence of persistent exchange between the Arctic Ocean and the Nordic Seas and other ocean basins during the late glacial. In addition, the similar signatures of elevated [CO_3^{2-}] and lower $\delta^{13}C$ during the late glacial in the subpolar North Atlantic between 2000–3000 m water depth and the northern Nordic Seas is a strong indication that the Nordic Seas may have contributed significantly to the lower glacial North Atlantic intermediate water. Altogether, our results indicate that during the late glacial the Atlantic water thickened and deepened to at least 2600 m water depth and flowed as a subsurface intermediate layer in the Nordic Seas and the Arctic Ocean with active overflows to the North Atlantic Ocean likely via the Denmark Strait. Open ocean convection in the Nordic seas probably ceased or became intermittent.

Finally, evidence from previous studies suggests enhanced terrestrial carbon flux to the northern Nordic Seas at the Heinrich stadial/interstadial 2 transition (~23.5 ka).

Comparing our [CO_3^{2-}] and $\delta^{13}C$ records with carbon cycle model results, we conclude that either the total subglacial or permafrost carbon release either was low or slow, or released directly to the atmosphere.

Figure & Table Captions

Figure 1. Map showing major ocean currents in the Nordic Seas and Arctic Ocean and the location of sediment cores. Yellow dots refer to the location of sediment cores from this study (HH12-946MC and HH12-948MC, Ezat et al., 2019) and puslished records discussed in this study (HLY0503-18TC, e.g., Cronin et al., 2012; 1294-4 and 1295-5, Hebbeln et al., 1994; PS1243 and MD99-2276, e.g., Thornalley et al., 2015; HM52-43, Veum et al., 1992). Atlantic water inflow is indicated by solid red arrows (surface inflow) and dashed red arrows (submerged inflow). Freshwater circulation are shown by white arrows. Nordic Seas overflows are indicated by black arrows.

Figure 2. Benthic $\delta^{18}O$ records from the Nordic Seas. Southern Norwegian Sea (red curve; Veum et al., 1992), central Nordic Seas (blue curves; Bauch et al., 2001) and Fram Strait records HH12-946MC (purple curves), HH12-948MC (black curves) (Ezat et al., 2019; this study). Numbers in plot **(c)** are un-calibrated ^{14}C dates obtained on *C. wuellerstorfi* (italic, underlined font) and *O. umbonatus* (normal font). Triangles in **(d)** shows $\delta^{18}O$ in *C. wuellerstorfi* after extensive acid leaching. Grey and orange highlighting refer to the Last Glacial Maximum (LGM) and the Holocene, respectively.

Figure 3. Deep Fram Strait, central Nordic Seas and Arctic Ocean temperature and $\delta^{18}O$ during the last glacial period. (a) $\delta^{18}O$ in *O. umbonatus* from Fram Strait records HH12-946MC (circles; Ezat et al., 2019; this study), HH12-948MC (triangles; Ezat et al., 2019) and Central Nordic Seas core MD99-2276 (squares; Thornalley et al., 2015). **(b)** Deep ocean temperature based on Mg/Ca in *O. umbonatus* from cores core MD99-2276 (squares; Thornalley et al., 2015), HH12-946MC (circles) andHH12-948MC (triangles). Error bars represent the combined 'analytical' (based on 2 s.d. of replicate measurements of in-house standard) and 'calibration' uncertainties. **(c)** Deep ocean temperature based on Mg/Ca in ostracods from the central Arctic Ocean, core HLY0503-18TC (Cronin et al., 2012). **(d)** Seawater $\delta^{18}O$ based on Mg/Ca and $\delta^{18}O$ in *O. umbonatus* from cores HH12-946MC (circles, this study), HH12-948MC (triangles, this study) and core MD99-2276 (squares, Thornalley et al., 2015). Dashed line represents average global ocean $\delta^{18}O$ following Spratt and Lisiecki (2016). **(e)** Planktic $\delta^{18}O$ records from the southern Norwegian Sea (red, core HM52-43, Veum et al., 1992), central Nordic Seas (dark green, core PS1243, Bauch et al., 2001; green, core MD99-2276, Thornalley et al., 2015), and Fram Strait (blue, HH12-946MC; light blue, HH12-948MC; Ezat et al., 2019 and this study). Red arrows above the x-axis refer to the location of the calibrated planktic ^{14}C dates that have been used in the age model of core HH12-946MC.

Figure 4. Evolution of deep ocean chemistry in Fram Strait and subpolar North Atlantic Ocean. (a) Deep ocean temperature from Fram Strait records HH12-946MC (circles), HH12-948MC (triangles). **(b)** B/Ca in *O. umbonatus* from cores HH12-946MC (circles) and HH12-948MC (triangles). Errors bars are based on 2 s.e. of replicate measurements of in-house standard (see Methods). **(c)** $\delta^{13}C$ in *O. umbonatus* from cores HH12-946MC (circles) and HH12-948MC (triangles). **(d)** $\delta^{13}C$ in organic matter from the Fram Strait records 1295-5

(dashed line and open circles) and 1294-4 (solid line and filled circles) (Hebbeln et al., 1994). **(e)** Carbonate ion concentration based on B/Ca measured in from core NEAP 8K (Yu et al., 2008). **(f)** $\delta^{13}C$ measured in *C. wuellerstorfi* from core NEAP 8K (Yu et al., 2008). **(g)** Atmospheric pCO_2 from Antarctic ice cores (Bereiter et al., 2015 and references therein).

Figure 5. Modeled changes in deep 'Northern Component Water' from idealized circulation changes (blue line) and carbon addition (0–88 Pg C; 1 Pg C= 10^{15} gram carbon) scenarios (black lines). The model results from the 'direct carbon addition to the atmosphere' and the 'carbon addition to the deep North Atlantic' experiments are shown (black lines) at the left and right panels, respectively. Abbreviations: GNAIW, Glacial North Atlantic Intermediate Water; HS, Heinrich Stadial; NADW, North Atlantic Deep Water.

Table 1. Radiocarbon dates on *Neogloboquadrina pachyderma, Cibicidoides wuellerstorfi* and *Oridorsalis umbonatus* from core HH12-946MC. Grey-highlighting indicates samples measured by 'gas source-based techniques' (this study; see Methods), while other samples were measured by 'graphitization-based' methodology (Ezat et al., 2019).

Acknowledgement

MME is funded by the Research Council of Norway and the Co-funding of Regional, National, and International Programmes (COFUND) – Marie Skłodowska-Curie Actions under the EU Seventh Framework Programme (FP7), project number 274429, and the Research Council of Norway through its Centres of Excellence funding scheme, grant number 223259. No potential financial conflicts of interests were reported by the authors. We thank

Dierk Hebbeln and Thomas Cronin for providing published data from the Fram Strait (cores 1294-4 and 1295-5) and Central Arctic Ocean (core HLY0503-18TC), respectively. We thank Leonid Polyak for helpful discussions.

Data availability statement

The new data presented in this article are available in the 'Supporting Information' and will be available at Zenodo database upon acceptance of this manuscript, DOI: https://doi.org/10.5281/zenodo.4436094.

References

Bard, E., Hamelin, B., & Fairbanks, R. G. (1990), U-Th ages obtained by mass spectrometry in corals from Barbados: sea level during the past 130,000 years. *Nature, 346*, 456–458.

Barker, S., Cacho, I., Benway, H., & Tachikawa, K. (2005), Planktonic foraminiferal Mg/Ca as a proxy for past oceanic temperatures: a methodological overview and data compilation for the Last Glacial Maximum. *Quaternary Science Reviews, 24*, 821–834.

Barker, S., et al. (2011), 800,000 years of abrupt climate variability. *Science, 334*, 347–351.

Barrientos, N., et al. (2018), Arctic Ocean benthic foraminifera Mg/Ca ratios and global Mg/Ca-temperature calibrations: New constraints at low temperatures. *Geochimica et Cosmochimica Acta 236*, 240–259.

Bauch, H.A., Erlenkeuser, H., Spielhagen, R.F., Struck, U., Matthiessen, J, Thiede, J., & Heinemeier, J. (2001), A multiproxy reconstruction of the evolution of deep and surface waters in the subarctic Nordic seas over the last 30,000 yr. *Quaternary Science Reviews, 20*, 659–678.

Bauska, T. K., Brook, E. J., Marcott, S. A., Baggenstos, D., Shackleton, S., Severinghaus, J. P., & Petrenko, V. V. (2018), Controls on millennial-scale atmospheric CO2 variability during the last glacial period. *Geophysical Research Letters, 45*, 7731–7740.

Bemis, B. E., Spero, H. J., Bijma, J., & Lea, D. W. (1998), Reevaluation of the oxygen isotopic composition of planktonic foraminifera: Experimental results and revised paleotemperature equations. *Paleoceanography, 13*, 150–160.

Bereiter, B., et al. (2015), Revision of the EPICA Dome C CO_2 record from 800 to 600 kyr before present. *Geophysical Research Letters, 42*, 542–549.

Bjørk, A. A., et al. (2012), An aerial view of 80 years of climate-related glacier fluctuations in southeast Greenland. *Nature Geoscience, 5*, 427–432.

612 Boyle, E. A., & Keigwin, L. D. (1985), Comparison of Atlantic and Pacific paleochemical
613 records for the last 215,000 years: Changes in deep ocean circulation and chemical
614 inventories. *Earth and Planetary Science Letters, 76*, 135–150.
615 Broecker, W. S. (1998), Paleocean circulation during the last deglaciation: a bipolar seesaw?.
616 *Paleoceanography, 13*, 119–121.
617 Broecker, W.S., Peng, T.H. (1982), *Tracers in the Sea*.
618 Butzin, M., Heaton, T. J., Köhler, P., & Lohmann, G. (2020), A short note on marine reservoir
619 age simulations used in IntCal20. *Radiocarbon*, 1–7.
620 Clark, P.U., Dyke, A.S., Shakun, J.D., Carlson, A.E., Clark, J., Wohlfarth, B., Mitrovica, J.X.,
621 Hostetler, S.W., & McCabe, A.M. (2009), The last glacial maximum. *Science, 325*,
622 710–714.
623 Corliss, B. H. (1985), Microhabitats of benthic foraminifera within deep-sea sediments.
624 *Nature, 314*, 435–438.
625 Cronin, T. M., et al. (2012), Deep Arctic Ocean warming during the last glacial cycle. Nature
626 Geoscience 5, 631–634.
627 Dansgaard, W., et al. (1993), Evidence for general instability of past climate from a 250-kyr
628 ice-core record. *Nature, 364*, 218–220.
629 Duplessy, J. C., Shackleton, N. J., Fairbanks, R. G., Labeyrie, L., Oppo, D., & Kallel, N.
630 (1988), Deepwater source variations during the last climatic cycle and their impact
631 on the global deepwater circulation. *Paleoceanography, 3*, 343–360.
632 Elderfield, H., Yu, J., Anand, P., Kiefer, T., & Nyland, B. (2006), Calibrations for benthic
633 foraminiferal Mg/Ca paleothermometry and the carbonate ion hypothesis. *Earth and*
634 *Planetary Science Letters, 250*, 633–649.
635 Ezat, M. M., Rasmussen, T. L., & Groeneveld, J. (2014), Persistent intermediate water
636 warming during cold stadials in the southeastern Nordic seas during the past 65 ky.
637 *Geology, 42*, 663–666.
638 Ezat, M. M., Rasmussen, T. L., Hönisch, B., Groeneveld, J., & Demenocal, P. (2017),
639 Episodic release of CO_2 from the high-latitude North Atlantic Ocean during the last
640 135 kyr. *Nature communications, 8*, 1–10.
641 Ezat, M. M., Rasmussen, T. L., Skinner, L. C., & Zamelczyk, K. (2019), Deep ocean ^{14}C
642 ventilation age reconstructions from the Arctic Mediterranean reassessed. Earth and
643 Planetary Science Letters 518, 67–75.
644 Fischer, H., et al. (2010), The role of Southern Ocean processes on orbital and millennial CO2
645 variations: A synthesis. *Quaternary Science Reviews, 29*, 193–205.
646 Gottschalk, J., Szidat, S., Michel, E., Mazaud, A., Salazar, G., Battaglia, M., Lippold, J., &
647 Jaccard, S.L. (2018), Radiocarbon Measurements of Small-Size Foraminiferal
648 Samples with the Mini Carbon Dating System (MICADAS) at the University of
649 Bern: Implications for Paleoclimate Reconstructions. *Radiocarbon, 60*, 469–491.
650 Hain, M. P., Sigman, D. M., & Haug, G. H. (2014), Distinct roles of the Southern Ocean and
651 North Atlantic in the deglacial atmospheric radiocarbon decline. *Earth and Planetary*
652 *Science Letters, 394*, 198–208.
653 Hain, M. P., Sigman, D. M., & Haug, G. H. (2010), Carbon dioxide effects of Antarctic
654 stratification, North Atlantic Intermediate Water formation, and subantarctic nutrient
655 drawdown during the last ice age: Diagnosis and synthesis in a geochemical box
656 model. *Global Biogeochemical Cycles, 24*.
657 Hansen, B., & Østerhus, S. (2000), North Atlantic–Nordic seas exchanges. *Progress in*
658 *Oceanography, 45*, 109–208.
659 Hanslik, D., Jakobsson, M., Backman, J., Björck, S., Sellén, E., O'Regan, M., Fornaciari, E.
660 and & Skog, G. (2010), Quaternary Arctic Ocean sea ice variations and radiocarbon
661 reservoir age corrections. *Quaternary Science Reviews, 29*, 3430–3441.

Heaton, T. J., et al (2020), Marine20—the marine radiocarbon age calibration curve (0–55,000 cal BP). *Radiocarbon, 62*, 779–820.
Hebbeln, D., Dokken, T., Andersen, E.S., Hald, M., & Elverhøi, A. (1994), Moisture supply for northern ice-sheet growth during the Last Glacial Maximum. *Nature, 370*, 357.
Huber, C., et al. (2006), Isotope calibrated Greenland temperature record over Marine Isotope Stage 3 and its relation to CH_4. *Earth and Planetary Science Letters, 243*, 504–519.
Jensen, M. F., Nisancioglu, K. H., & Spall, M. A. (2018), Large changes in sea ice triggered by small changes in Atlantic water temperature. *Journal of Climate, 31*, 4847–4863.
Jessen, S. P., Rasmussen, T. L., Nielsen, T., & Solheim, A. (2010), A new Late Weichselian and Holocene marine chronology for the western Svalbard slope 30,000–0 cal years BP. *Quaternary Science Reviews, 29*, 1301–1312.
Knies, J., et al. (2018), Nordic Seas polynyas and their role in preconditioning marine productivity during the Last Glacial Maximum. *Nature communications, 9*, 1–10.
Köhler, P., Knorr, G., & Bard, E. (2014), Permafrost thawing as a possible source of abrupt carbon release at the onset of the Bølling/Allerød. *Nature communications, 5*, 1–10.
Lind, S., Ingvaldsen, R. B., & Furevik, T. (2018), Arctic warming hotspot in the northern Barents Sea linked to declining sea-ice import. *Nature climate change, 8*, 634–639.
Luckman, A., Murray, T., De Lange, R., & Hanna, E. (2006), Rapid and synchronous ice-dynamic changes in East Greenland. *Geophysical Research Letters, 33*.
Mackensen, A., & Schmiedl, G. (2019), Stable carbon isotopes in paleoceanography: Atmosphere, oceans, and sediments. *Earth-Science Reviews, 102893*.
Mankoff, K. D., Solgaard, A., Colgan, W., Ahlstrøm, A. P., Khan, S. A., & Fausto, R. S. (2020), Greenland Ice Sheet solid ice discharge from 1986 through March 2020. *Earth System Science Data, 12*, 1367–1383.
Marcott, S. A., et al. (2014), Centennial-scale changes in the global carbon cycle during the last deglaciation. *Nature, 514*, 616–619.
Meyer, V. D., Hefter, J., Köhler, P., Tiedemann, R., Gersonde, R., Wacker, L., & Mollenhauer, G. (2019), Permafrost-carbon mobilization in Beringia caused by deglacial meltwater runoff, sea-level rise and warming. *Environmental Research Letters, 14(8)*, 085003.Misra, S., Greaves, M., Owen, R., Kerr, J., Elmore, A. C., & Elderfield, H. (2014), Determination of B/Ca of natural carbonates by HR-ICP-MS. *Geochemistry, Geophysics, Geosystems, 15*, 1617–1628.
Murray, J. W. (2006), Ecology and applications of benthic foraminifera. *Cambridge University Press*.
Pena, L. D., Calvo, E., Cacho, I., Eggins, S., & Pelejero, C. (2005), Identification and removal of Mn-Mg-rich contaminant phases on foraminiferal tests: Implications for Mg/Ca past temperature reconstructions. *Geochemistry, Geophysics, Geosystems, 6*.
Peng, T. H., & Broecker, W. S. (1984), The impacts of bioturbation on the age difference between benthic and planktonic foraminifera in deep sea sediments. *Nuclear Instruments and Methods in Physics Research Section B: Beam Interactions with Materials and Atoms, 5*, 346–352.
Rae, J. W., et al. (2018), CO_2 storage and release in the deep Southern Ocean on millennial to centennial timescales. *Nature, 562*, 569–573.
Rae, J. W., Foster, G. L., Schmidt, D. N., & Elliott, T. (2011), Boron isotopes and B/Ca in benthic foraminifera: Proxies for the deep ocean carbonate system. *Earth and Planetary Science Letters, 302*, 403–413.
Rasmussen, T. L., & Thomsen, E. (2004), The role of the North Atlantic Drift in the millennial timescale glacial climate fluctuations. *Palaeogeography, Palaeoclimatology, Palaeoecology, 210*, 101–116.

Rysgaard, S., Bendtsen, J., Pedersen, L. T., Ramlov, H. & Glud, R. N. (2009), Increased CO_2 uptake due to sea ice growth and decay in the Nordic Seas. *Journal of Geophysical Research: Oceans, 114*, C09011.

Shackleton, N. J. (1974), Attainment of isotopic equilibrium between ocean water and the benthonic foraminifera genus Uvigerina: isotopic changes in the ocean during the last glacial.

Sigman, D. M., Hain, M. P., & Haug, G. H. (2010), The polar ocean and glacial cycles in atmospheric CO_2 concentration. *Nature, 466*, 47–55.

Sigman, D. M., Lehman, S. J., & Oppo, D. W. (2003), Evaluating mechanisms of nutrient depletion and 13C enrichment in the intermediate-depth Atlantic during the last ice age. *Paleoceanography, 18*.

Stuiver, M., Reimer, P.J., and Reimer, R.W., 2020, CALIB 8.2 [WWW program] at http://calib.org.

Szidat, S., Salazar, G. A., Vogel, E., Battaglia, M., Wacker, L., Synal, H. A., & Türler, A. (2014), ^{14}C analysis and sample preparation at the new Bern Laboratory for the Analysis of Radiocarbon with AMS (LARA). *Radiocarbon, 56*, 561–566.

Tarnocai, C., Canadell, J. G., Schuur, E. A., Kuhry, P., Mazhitova, G., & Zimov, S. (2009), Soil organic carbon pools in the northern circumpolar permafrost region. *Global biogeochemical cycles, 23*.

Thornalley, D.J.R., Bauch, H.A., Gebbie, G., Guo, W., Ziegler, M., Bernasconi, S.M., Barker, S., Skinner, L.C., & Yu, J. (2015), A warm and poorly ventilated deep Arctic Mediterranean during the last glacial period. *Science, 349*, 706–710.

Tisserand, A. A., Dokken, T. M., Waelbroeck, C., Gherardi, J. M., Scao, V., Fontanier, C., & Jorissen, F. (2013), Refining benthic foraminiferal Mg/Ca-temperature calibrations using core-tops from the western tropical Atlantic: Implication for paleotemperature estimation. *Geochemistry, Geophysics, Geosystems, 14*, 929–946.

Veum, T., Jansen, E., Arnold, M., Beyer, I., & Duplessy, J.C. (1992), Water mass exchange between the North Atlantic and the Norwegian Sea during the past 28,000 years. *Nature, 356*, 783.

Vonk, J. E., et al. (2012), Activation of old carbon by erosion of coastal and subsea permafrost in Arctic Siberia. *Nature, 489*, 137–140.

Wadham, J. L., et al. (2019), Ice sheets matter for the global carbon cycle. *Nature communications, 10*, 1–17.

Yu, J., & Elderfield, H. (2007), Benthic foraminiferal B/Ca ratios reflect deep water carbonate saturation state. *Earth and Planetary Science Letters, 258*, 73–86.

Yu, J., et al. (2020), Last glacial atmospheric CO_2 decline due to widespread Pacific deep-water expansion. *Nature Geoscience, 13*, 628–-633.

Yu, J., Broecker, W. S., Elderfield, H., Jin, Z., McManus, J., & Zhang, F. (2010), Loss of carbon from the deep sea since the Last Glacial Maximum. *Science, 330*, 1084–1087.

Yu, J., et al. (2016), Sequestration of carbon in the deep Atlantic during the last glaciation. *Nature Geoscience, 9*, 319–324.

Yu, J., Elderfield, H., & Piotrowski, A. M. (2008), Seawater carbonate ion-δ13C systematics and application to glacial–interglacial North Atlantic ocean circulation. *Earth and Planetary Science Letters, 271*, 209–220.

Zamelczyk, K., Rasmussen, T.L., Husum, K., Godtliebsen, F., & Hald, M. (2014), Surface water conditions and calcium carbonate preservation in the Fram Strait during marine isotope stage 2, 28.8–15.4 kyr. *Paleoceanography, 29*, 1–12.

Figure 1.

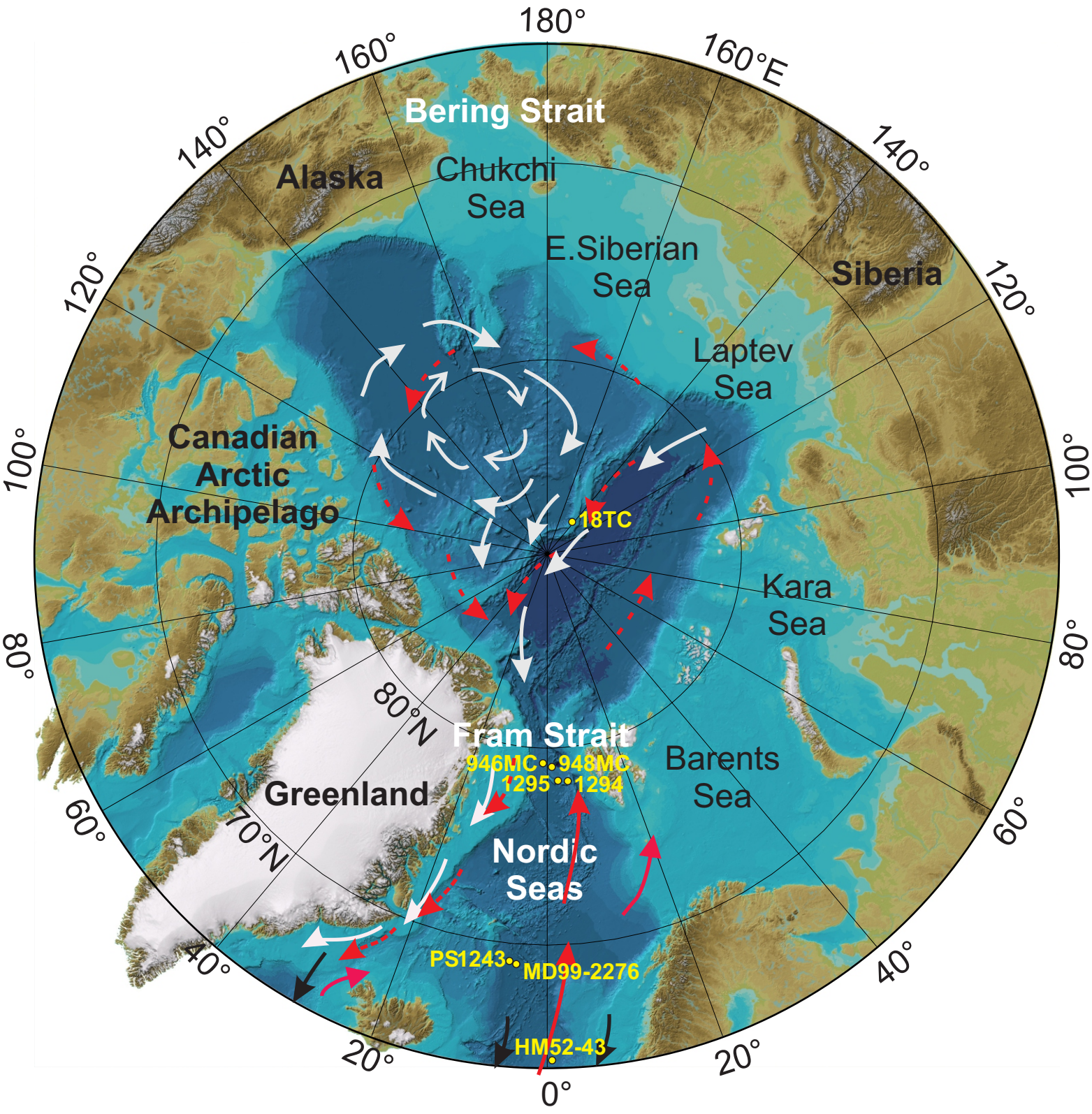
180°
160°
160°E
140°
140°
120°
120°
100°
100°
80°
80°
60°
60°
40°
40°
20°
20°
0°
Bering Strait
Alaska
Chukchi Sea
E.Siberian Sea
Siberia
Laptev Sea
Canadian Arctic Archipelago
18TC
Kara Sea
80°N
Fram Strait
946MC
948MC
1295
1294
Barents Sea
Greenland
70°N
Nordic Seas
PS1243
MD99-2276
HM52-43

Figure 2.

● *C. wuellerstorfi* □ *O. umbonatus*

△ Leached *C. wuellerstorfi*

Fram Strait

HH12-948MC

HH12-946MC

14460 14517 15172 18335 18787 18511 19232

Central Nordic Seas

PS1243

Southern Norwegian Sea

HM52-43

Benthic $\delta^{18}O$ (‰)

3.2

4

4.8

a

b

c

d

0 10 20 30

Age (ka)

Figure 3.

Holocene
HS1
LGM
MIS 3
e
Planktic δ18O (‰)
2
3
4
5
d
Deep sea δ18O (‰)
1.2
0.8
0.4
0
c
BWT (°C) Deep central Arctic
2
1.5
1
0.5
0
-0.5
b
BWT (°C) Deep Nordic Seas
1.5
1
0.5
0
-0.5
-1
-1.5
a
Benthic δ18O (‰)
4
4.4
4.8
0
10
20
30
40
Age (ka)

Figure 4.

Holocene
LGM
MIS 3
IS 2
HS 2
Atmosphere
280
240
200
Atmospheric pCO_2 (ppm)
g
N. North Atlantic (2360 m depth)
1.2
0.8
0.4
Epifaunal Benthic $\delta^{13}C$ (‰)
f
e
$[CO_3^{2-}]$ (µmol/kg)
140
130
120
110
100
Fram Strait (~2600 m depth)
Increased terrestrial carbon
-22
-23
-24
-25
-26
Organic matter $\delta^{13}C$ (‰)
d
c
Infaunal Benthic $\delta^{13}C$ (‰)
0
-1
-2
Higher $[CO_3^{2-}]$
70
60
50
40
Infaunal Benthic B/Ca (µmol/mol)
b
a
BWT (°C)
1
0
-1
0
5
10
15
20
25
30
35
40
Age (ka)

Figure 5.

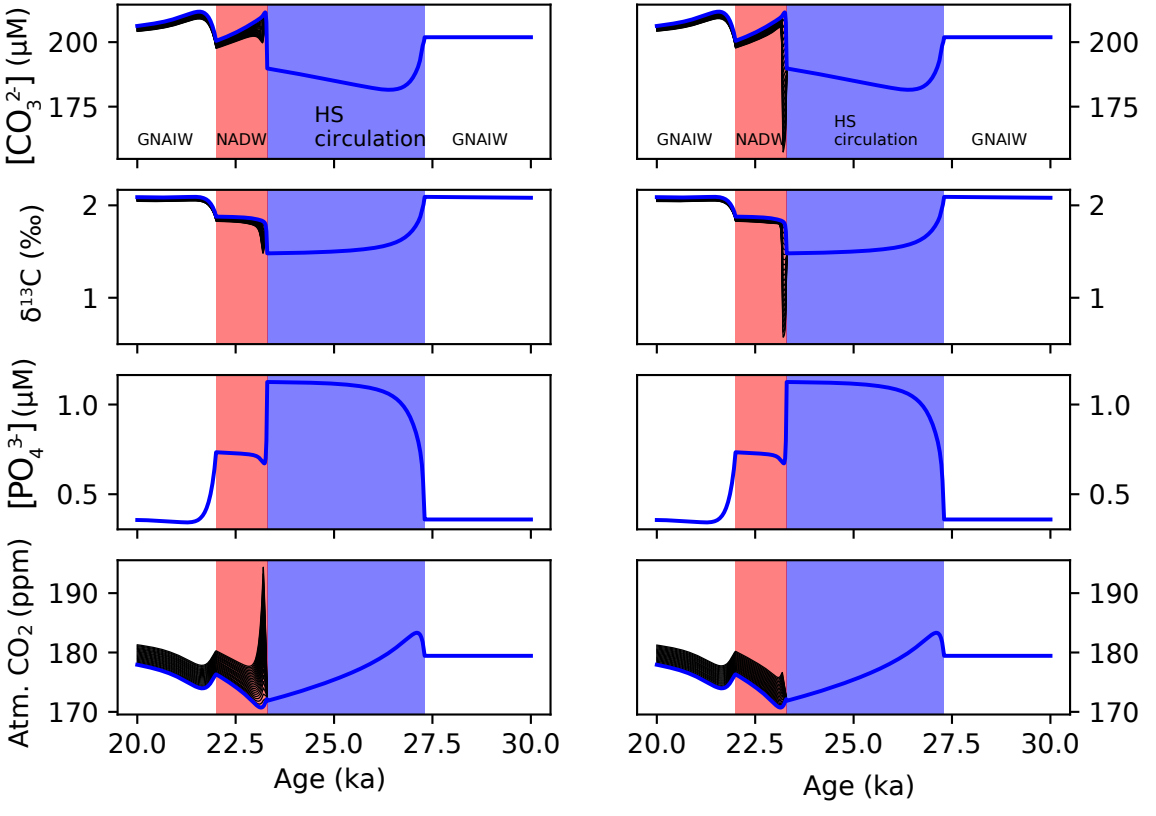
[CO3 2-] (μM)
200
175
GNAIW
NADW
HS
circulation
GNAIW
δ13C (‰)
2
1
[PO4 3-] (μM)
1.0
0.5
Atm. CO2 (ppm)
190
180
170
20.0
22.5
25.0
27.5
30.0
Age (ka)

Sediment Depth (cm)	Calendar Age (ka)	^{14}C Age (years BP)		
		N. pachyderma	*C. wuellerstorfi*	*O. umbonatus*
25.25	19.7	18075 ±90		18580 ±88
25.75	20.1	18399 ±75		18511 ±82
27.25	20.6	18765 ±73	14460 ±190	18787 ±95
28.25	21.2	19335 ±77	14206 ±205	19232 ±148
29.25	22.6	19833 ±284	15175 ±169	
29.75	23.3		15372 ±205	
30.75	24.7	22372 ±108		
32.75	25.5	23076 ±131		25327 ±161
33.75	27.1	24741 ±134		26118 ±170
35.75	30.7	28333 ±225		29715 ±340